2011 IEEE International Conference on Robotics and Automation
Shanghai International Conference Center
May 9-13, 2011, Shanghai, China

The ParkourBot – A Dynamic BowLeg Climbing Robot

Amir Degani, Siyuan Feng, H. Benjamin Brown, Kevin M. Lynch, Howie Choset and Matthew T. Mason

***Abstract*— The ParkourBot is an efficient and dynamic climbing robot. The robot comprises two springy legs connected to a body. Leg angle and spring tension are independently controlled. The robot climbs between two parallel walls by leaping from one wall to the other. During flight, the robot stores elastic energy in its springy legs and automatically releases the energy to "kick off" the wall during touch down. This paper elaborates on the mechanical design of the ParkourBot. We use a simple SLIP model to simulate the ParkourBot motion and stability. Finally, we detail experimental results, from open-loop climbing motions to closed-loop stabilization of climbing height in a planar, reduced gravity environment.**

I. Introduction

This work is inspired in part by the grace, efficiency, and adaptability of human parkour, sometimes known as free running. Parkour is the art of moving from place to place as quickly and efficiently as possible, overcoming obstacles using leaps, swings, rolls, and other dynamic movements. Whereas walls, chutes, and trenches are obstacles that may not be navigable using less dynamic forms of locomotion, in parkour these "obstacles" are potential sources of reaction forces for a well-placed hand or foot. For parkour practitioners ("traceurs") to make maximum use of these handholds and footholds, they must have precise control of their body dynamics. By taking advantage of dynamics, and by knowing the geometry and contact properties (e.g., friction and restitution) of the environment, the set of reachable states by parkour is vastly increased over that by more conventional locomotion.

To proceed efficiently over obstacles, the traceur stores energy elastically in muscles and tendons, and kinetically in translation and rotation. These energies can then be directed to move seamlessly from one task to the next. The climbing robot in this paper, called ParkourBot, is based on two dynamic robots which we have previously built. The first, the BowLeg hopper [1], [2], has high energy efficiency and requires feedback for stable hopping. The second, the DSAC – dynamic single actuator climber [3], [4], sacrifices energy efficiency for stable open-loop climbing of a chute. This paper describes the design and control of a biped BowLeg climber (Fig. 1) that inherits properties of the BowLeg hopper and the DSAC. The ParkourBot is designed to address different types of climbing tasks such as simple chutes and more complex environment having footholds at different orientations. The current paper focuses on climbing between two vertical walls with demonstrations in a planar, reduced gravity environment.

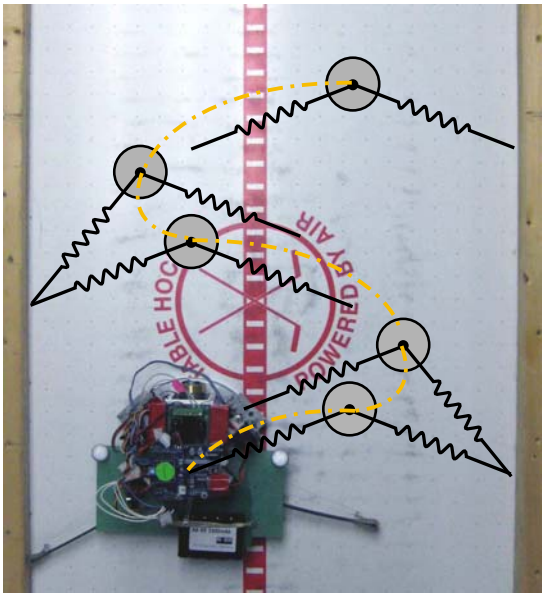

Fig. 1. Overlay of the ParkourBot climbing motion with the simplified SLIP model. The ParkourBot is on top of an inclined air-table, providing a reduced gravity, planar environment.

II. Related Work

This work is allied with previous work on dynamically locomoting robots, particularly hopping, passive dynamic walking, and running robots, with many legs or as few as one. The work of Raibert is particularly influential, as it demonstrated that simple control laws could be used to stabilize hopping and control the running speed and direction of 2D and 3D single-leg hoppers [5], [6]. To improve the energy efficiency of a hopping robot, Brown and Zeglin introduced the BowLeg hopper, which can traverse a series of stepping stones [1], [7], [2]. The BowLeg is a key design element in the current ParkourBot design.

To facilitate analysis and control design of running and walking robots, it is convenient to develop simplified models which nonetheless retain the essential character of the original physical system. Two examples are the spring-loaded inverted pendulum (SLIP) model of running robots [8], [9],

This work has been supported in part by NSF Grants IIS-08030826 and IIS-0803734 . This work does not necessarily reflect the position or the policy of the Government.

A. Degani, S. Feng, H.B. Brown, H. Choset and M.T. Mason are with the Robotics Institute, Carnegie Mellon University, 5000 Forbes Avenue, Pittsburgh, PA 15213 USA <adegani, hbb, choset, matt.mason>@cs.cmu.edu, sfeng@andrew.cmu.edu

K.M. Lynch is with the Mechanical Engineering Department, Northwestern University, Evanston, IL 60208 USA kmlynch@northwestern.edu

[10] and the "simplest walking model" [11]. Such models can be used to extract important relationships between design and control parameters and performance. For example, Kuo used the simplest walking model to demonstrate that applying an impulse at toe-off is a more energy-efficient way to inject energy into a walker than applying a torque to the stance leg [12]. In the current work, we develop a simplified model of the ParkourBot to analyze the open-loop dynamic stability in the chute-climbing task. Our chute-climbing task may be viewed as "vertical running," in that our goal is to stabilize a desired limit cycle motion, as in running robots.

Other dynamic multi-legged running robots include RHex [13], the Whegs (wheel-legs) robots [14], and Sprawlita [15]. These robots use compliant legs that allow them to both scramble over obstacles and locomote relatively efficiently on flat ground.

One aspect of this work that differs from the work described above is that locomotion occurs largely in the vertical direction. While a number of robots have been designed for climbing locomotion, they are mostly quasistatic. The Alicia3 robot climbs walls by using pneumatic adhesion at one or more of three "cups" connected by two links [16]. The climbing robots in [17], [18] climb by kinematic or quasistatic bracing between opposing walls. The four-limbed free-climbing LEMUR robot goes up climbing walls by choosing a sequence of footholds and motions that keep the robot in static equilibrium at all times [19]. Gecko-inspired directional dry adhesives allow Stickybot and Waalbot to climb vertical, smooth surfaces such as glass [20], [21], and the RiSE and SpinybotII robots climb soft or rough walls using spined feet to catch on asperities in the wall [22], [23]. Unlike the quasistatic climber, a few mechanisms [24], [25] have been proposed to achieve a vertical climbing task using dynamic motions while using spines to attach to carpeted surfaces. The current ParkourBot has no adhesives or clamping mechanisms and cannot maintain height statically. Like runners, we use dynamics and relay on reaction forces inside a friction cone, but unlike runners, our footholds, and desired net motion, are aligned with gravity.

III. Mechanical Design

As mentioned previously, this current ParkourBot is based on the BowLeg hopper [1]. However, in order to adapt it to a climbing scenario, we have decreased the size and have implemented a new mechanism design. This section will first explain the previous BowLeg concept and later review some of the new mechanism design components.

A. BowLeg design

The BowLeg [26], a robotic leg concept developed at Carnegie Mellon, integrates the functions of structure and spring into a lightweight leg. As shown in Fig. 2, the BowLeg resembles an archer's bow, with the hip joint at one end and the foot at the other end of the bow. Made of unidirectional fiberglass ("bow glass"), the BowLeg can store a large amount of elastic energy, typically enough to lift its own weight 50 meters vertically. The concept of a single-leg hopping machine using BowLeg technology is illustrated in Fig. 2. When the BowLeg hopper is in flight, a low-power actuator stores energy in the BowLeg by tensioning a string attached to the foot. A separate actuator uses control strings to position the leg for the next impact. Upon impact, the string becomes slack and the BowLeg quickly releases its stored energy. The leg rotates freely about a hip joint, so that the foot matches ground speed without actuation, and no attitude-disturbing torque is transmitted through the joint. Hopping motion is controlled by choosing the angle of the leg at impact and the amount of energy stored in the BowLeg during flight. A special clutch mechanism (Fig. 3) is used to release the leg when impact with the floor occurs.

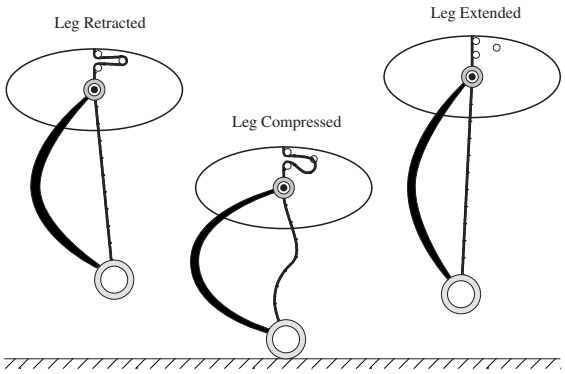

Fig. 2. Schematics of the BowLeg monopod (reprinted with permission from [2]).

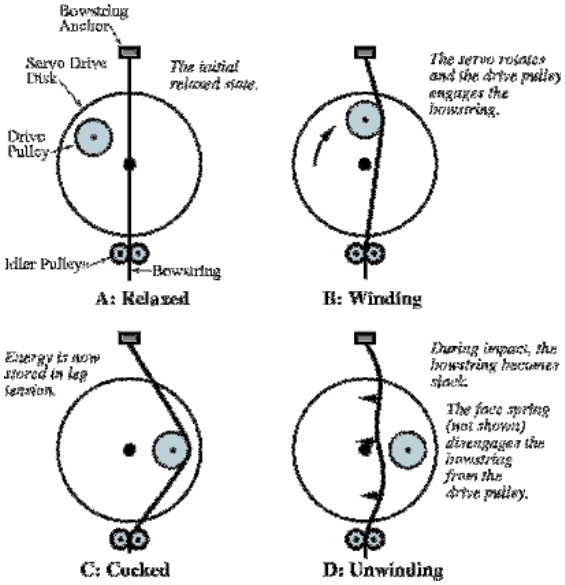

Fig. 3. Schematic of the prototype thrust mechanism which stores energy in the leg during flight. The cycle begins in the relaxed state (A). During winding (B), the servo disk rotates, the drive pulley engages the bowstring, and the displacement of the bowstring compresses the leg (not shown). The energy stored in the cocked position (C) is a function of rotation angle. During the impact (D), the string goes slack, the face spring (not shown) nudges the bowstring off the pulley, and the leg extends to full length. Not shown are the servo body or the leg. The winding direction and string displacement alternate left-right. Reprinted from [1] ©[1998 IEEE].

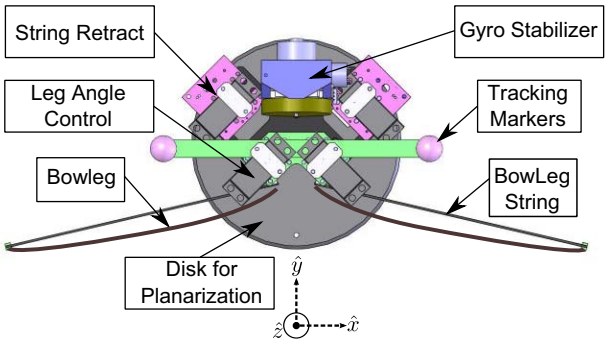

Fig. 4. CAD design of the ParkourBot mechanism.

B. ParkourBot design overview

The current ParkourBot depicted in Fig. 4 comprises five primary parts: disk, BowLeg, leg angle control mechanism, retract mechanism, and a gyro-stabilizer. The disk, the main body of the robot, floats on top of an inclined air-table in order to planarize the system while enabling lower effective gravity. The BowLeg includes a thin, unidirectional fiberglass strip that provides the main leg structure and elastic energy storage; the hip lever that softens the leg stiffness and connects to the hip; the bow string that passes through the hip, connecting the foot to the retract mechanism; and a rubber foot pad that enhances foot traction. The remaining parts of the climber are described below.

C. Retract mechanism

The retract mechanism pulls on the bow string and stores potential energy in the springy BowLeg. It also includes a clutch to release the spring energy when the string goes slack during stance. As shown for the BowLeg Hopper in Fig. 3, when the leg contacts the wall, the string slackens and the clutch disengages the string from the retract arm. This enables the BowLeg to fully extend and "kick" the wall. The initial design of the retract mechanism for the climber was a miniature version of this, but reliable release of the string could not be achieved at the smaller scale. A new mechanism was conceived and built, as shown in Fig. 5. In the current design, a telescoping slider (green) engages the driven arm (orange) when the string is under tension, allowing the arms to move together, pull the string and retract the leg. When the string goes slack due to foot contact with the wall, the slider retracts and disengages from the drive arm, releasing the stored energy when the foot lifts off the wall.

D. Gyro-stabilizer

To maintain a constant orientation of the main body of the robot in the $\hat{z}$ direction, we have implemented a gyro-stabilizer. The gyro-stabilizer is a fast spinning flywheel mounted on a single-axis gimbal. The gyro spin axis is nominally aligned with the air table surface and the "vertical" axis ($\hat{y}$) of the climber. The gimbal permits the gyro to precess about the $\hat{x}$-axis, stabilizing the attitude about the $\hat{z}$-axis. A motor and potentiometer attached to the gimbal axis allow active correction of the body orientation. In our experiments, where the goal is to keep the body orientation constant, such corrections are rarely needed.

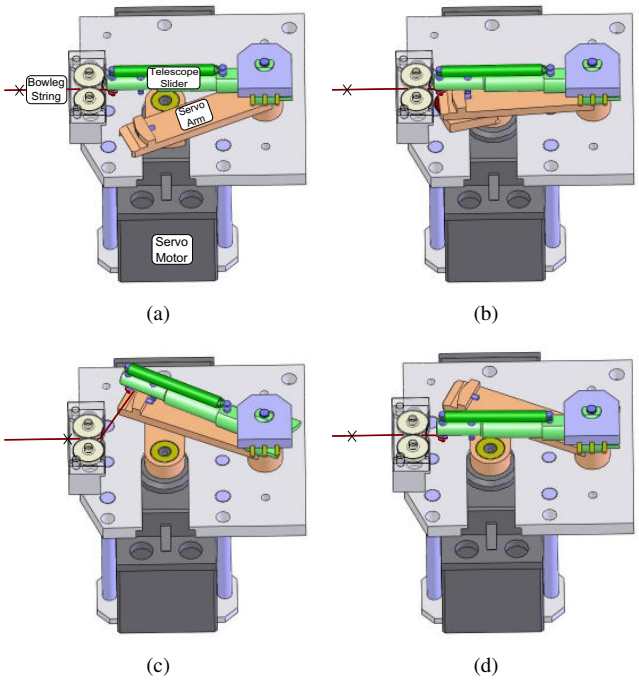

Fig. 5. Retract mechanism sequence. The string is marked with an 'x' for length reference. (a) Leg extended, telescope slider fully extended. (b) Servo arm rotates and engages (couples) with latch pin. (c) Servo arm and telescope slider rotate together to retract leg. After wall impact, string goes slack and the spring pulls the telescope slider back. This causes the latch pin to disengage. (d) The telescope slider is pulled back to center by tension in the bow string. While leg extends and tension builds back in the string, the telescope slider extends and the sequence repeats.

IV. Modeling

A two-legged SLIP model is used for our mechanism. Two massless legs with rest length l_0 and stiffness k are attached to a point mass m as in Fig. 6. Leg angle ψ_0 and leg length ζ_0 at touch down are the controls of the system, where $\zeta_0 \leq l_0$ determines the energy stored in the leg. Two parallel walls are at distance d apart, the gravitational acceleration is g and we assume no slip at contact. The inertial frame is centered between the walls. An entire stride of the SLIP model is composed of flight phase, touch down, stance phase, lift off and back to flight phase. Despite the simplicity of the model, during stance phase the system is a two degree-of-freedom Hamiltonian system without an explicit solution. Thus analysis and simulation in the later sections are done numerically in $Matlab^{TM}$.

During flight phase, the motion is ballistic and integrable, with configuration variables (x,y). During stance phase it is convenient to replace the cartesian coordinates with polar coordinates and represent the configuration as (ζ,ψ). Since the leg is massless, touch down occurs without impact when the end of the leg touches the ground. Lift off occurs when the leg length ζ reaches the spring resting length, l_0, and $\dot{\zeta}$ is positive. After liftoff the leg angle repositions back to ψ_0.

To better capture the physical system, we add two damping terms to the stance phase equations of motion, c_ζ and c_ψ,

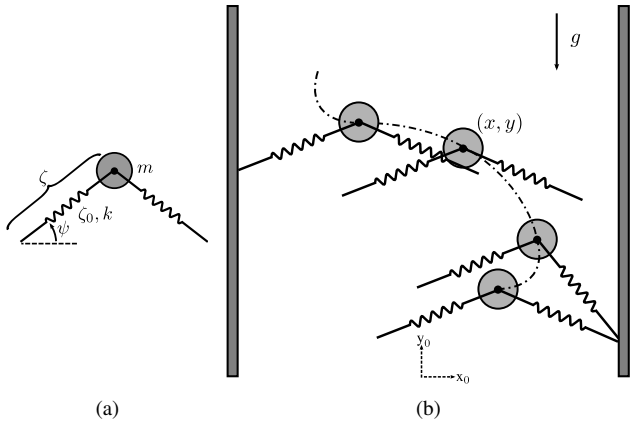

(a) (b)

Fig. 6. Mechanism schematics and configuration variables: (a) configuration variables during stance phase; (b) one full sequence including touch down on right wall, stance phase and flight phase toward left wall.

TABLE I

PARAMETERS FOR ANALYSIS AND EXPERIMENT SECTIONS

Dimensional Parameters		
Parameter	Description	Value
m	body mass	1.54 kg
l_0	leg rest length	0.223 m
d	wall width	0.54 m
k	leg spring stiffness	525 $\frac{\text{N}}{\text{m}}$
g	gravitational acceleration	0.98 $\frac{\text{m}}{\text{s}^2}$
c_ζ	damping coef.	1 $\frac{\text{Ns}}{\text{m}}$
c_ψ	damping coef.	1 Ns
Nondimensional Parameters		
α	nondimensional (ND) force - $\frac{kl_0}{mg}$	77.57
$\hat{d}$	ND wall width - $\frac{d}{\zeta_0}$	2.42
$\hat{c}_\zeta$	Damping coef. - $\frac{c_\zeta}{\sqrt{g/l_0}}$	0.4770
$\hat{c}_\psi$	Damping coef. - $\frac{c_\psi}{g/l_0}$	0.2276

acting along the leg and at the pivot with the wall.

The Lagrangian in polar coordinates during stance phase is

$$L = \frac{1}{2}m(\dot{\zeta}^2 + \zeta^2\dot{\psi}^2) - \frac{k}{2}(l_0 - \zeta)^2 - mg\zeta\sin(\psi). \quad (1)$$

To find the nondimensional equations, we rescale with characteristic length l_0 and characteristic time $\sqrt{\frac{l_0}{g}}$. This converts the system into nondimensional variables $\hat{\zeta} = \frac{\zeta}{l_0}$, $\hat{\psi} = \psi$ and $\hat{t} = \sqrt{\frac{g}{l_0}}t$. The nondimensional Lagrangian becomes

$$\hat{L} = \frac{1}{2}mgl_0(\dot{\hat{\zeta}}^2 + \hat{\zeta}^2\dot{\hat{\psi}}^2) - \frac{k}{2}{l_0}^2(1 - \hat{\zeta})^2 - mgl_0\hat{\zeta}\sin(\hat{\psi}). \quad (2)$$

After adding viscous damping for both linear and rotational motion during stance phase we arrive at a set of nondimensional equations of motion

$$\begin{aligned} \ddot{\hat{\zeta}} &= \alpha - \alpha\hat{\zeta} + \hat{\zeta}\dot{\hat{\psi}}^2 - \sin(\hat{\psi}) - \hat{c}_\zeta\dot{\hat{\zeta}} \\ \ddot{\hat{\psi}} &= -\frac{1}{\hat{\zeta}}(\cos(\hat{\psi}) - 2\dot{\hat{\zeta}}\dot{\hat{\psi}}) - \hat{c}_\psi\dot{\hat{\psi}}, \end{aligned} \quad (3)$$

where $\alpha = \frac{kl_0}{mg}$ is the ratio between the maximum spring force and the gravitational force. The ratio α gets larger as the spring gets stiffer or gravity shrinks.

V. ANALYSIS AND SIMULATION

For the analysis section and the experimental section we use the parameters in Table I. The BowLeg spring coefficient, k, was empirically approximated by measuring the displacement to a known load. Damping coefficients, c_ζ and c_ψ, were approximated from experimental data and drop tests. In the experimental setup, limited leg thrust allowed climbing in effective gravity less than $2\frac{\text{m}}{\text{s}^2}$.

A. Poincaré map and Poincaré section

The bipedal SLIP model is a hybrid system characterized by separate continuous flows (flight / stance phase) connected by discrete transitions (touch down / lift off). We use a Poincaré map to convert the hybrid system into a discrete-time system. Using the symmetry of the system we "flip" coordinates during touch down at the right wall and define the Poincaré map as a jump from the left wall to the right wall back to stance phase at the left wall. We choose the Poincaré section at touch down after the coordinate "flip". The touch down position x is calculated from ζ_0 and ψ_0. The state variable y does not appear in the Poincaré section. We do not want to stabilize it, and due to the vertical symmetry it does not appear in the equations of motion for the other state variables. We are left with only two state variables, $\dot{x}$ and $\dot{y}$, in our Poincaré section.

B. Fixed-point and local stability

A period-n fixed-point is a point on the Poincaré section that is mapped back to itself after applying the Poincaré map $\mathbf{P}$ n times. To find a period-n fixed-point q^*, with the controls ζ_0 and ψ_0 fixed, we use the Levenberg-Marquardt gradient descent method ([27]) to find the zeros of $\mathbf{P}^n(q) - q$, where n is the periodicity of the desired fixed point, and q is the state on the Poincaré section. The gradient is calculated numerically.

To find the local stability of an orbit, we linearize around the fixed-point by computing a forward difference approximation to the Jacobian. A fixed-point is stable if and only if both of its eigenvalues are inside the unit circle in the complex plane.

In experiments, we have noticed an asymmetry of the two leg controls due to imperfection of the servo motor controller. To simulate this asymmetry, we introduce alternating controls (ψ_0 and ζ_0) between Poincaré maps. On odd jumps, ψ_{0L}, ζ_{0L} are used, while on even jumps, ψ_{0R}, ζ_{0R} are used. For the symmetric case with identical controls, we searched for stable period-1 motions. Depending on the fixed controls and the initial conditions of the search, we found representative stable period-1 gaits for descending, jumping in place, and climbing upwards. For the asymmetric case, we found stable period-2 and period-4 gaits for climbing, jumping in place, and descending. We did not search exhaustively for all stable gaits over all possible controls, and the solutions shown here are local attractors for particular gradient searches we tried. Fig. 7 depicts a stable period-1 gait for the symmetric case,

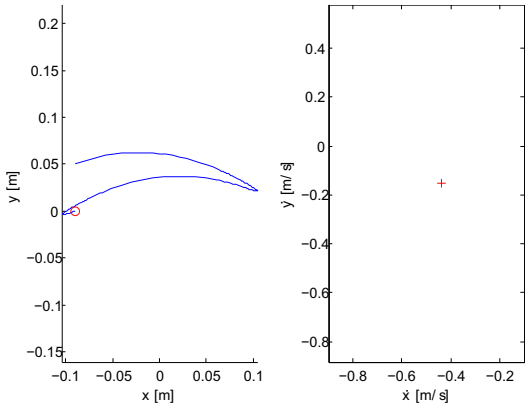

(a) stable period-1 with symmetric controls

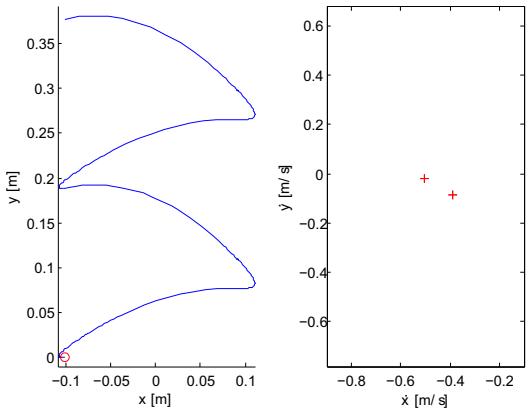

(b) stable period-2 with asymmetric controls

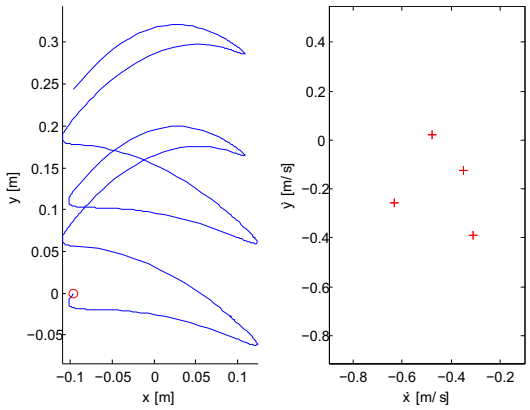

(c) stable period-4 with asymmetric controls

Fig. 7. Trajectories and fixed-points of stable gaits. Left column shows the trajectory of two cycles starting from a fixed-point (red circle), and right column shows the fixed-points on the Poincaré section (red '+'). The magnitudes of the maximum eigenvalues are 0.9007, 0.8652 and 0.5746 respectively. Controls: (a) $\psi_{0L} = \psi_{0R} = 30°$ and $\hat{\zeta}_{0L} = \hat{\zeta}_{0R} = 0.93$. (b) $\psi_{0L} = \psi_{0R} = 30°$, $\hat{\zeta}_{0L} = 0.87$ and $\hat{\zeta}_{0R} = 0.9$. (c) $\psi_{0L} = 30°$, $\psi_{0R} = 35°$, $\hat{\zeta}_{0L} = 0.9$ and $\hat{\zeta}_{0R} = 0.95$.

and stable period-2 and period-4 gaits for the asymmetric case.

C. Varying energy input

As Fig. 8 shows, there is a high correlation between energy input (the amount of leg retraction) and the stability of the system. Higher input energy corresponds to higher local stability and a larger basin of attraction. We vary the energy

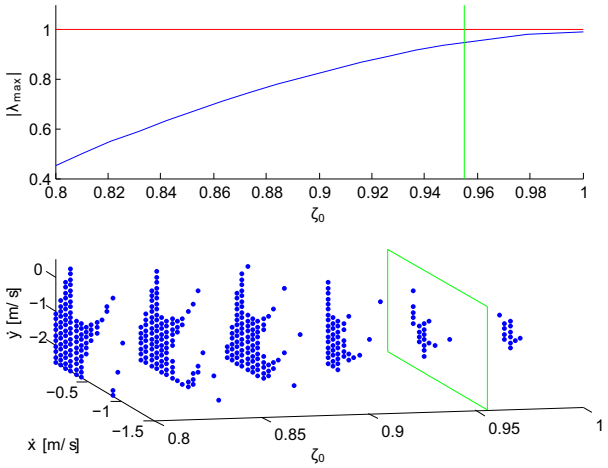

Fig. 8. Varying $\hat{\zeta}_0$ with symmetric controls. All fixed-points are period-1 motions. Green line / plane indicates critical $\hat{\zeta}_0$ for jumping in place, leg lengths to the right of green line / plane correspond to climbing down. Upper graph shows the maximum magnitude of eigenvalue of the Jacobian for the fixed-point given $\hat{\zeta}_0$. Lower graph shows the basin of attraction for various energy levels.

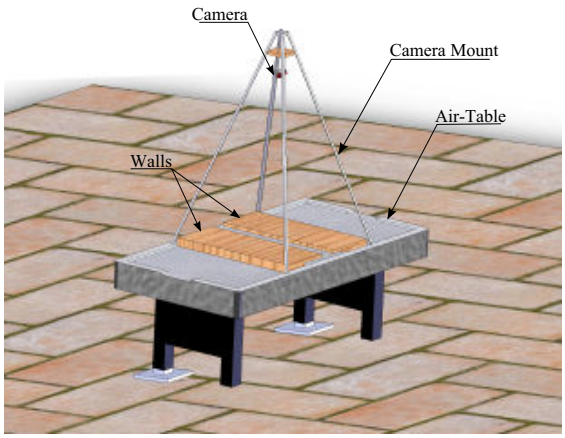

Fig. 9. Experimental setup: air table and tracking system.

input by changing the amount of leg retraction, then compute the basin of attraction and fixed-point for that particular leg retraction.

VI. Experiments

A. Experimental setup

We use a tilted air table (see Fig. 9) as the testbed, which enforces the planar constraint on the ParkourBot, and provides an easy way to change the effective gravity by tilting the table. Since the contact between the ParkourBot and the table is frictionless, this setup is equivalent to pure vertical climbing in a reduced gravity environment. Friction between the rubber foot and wall was observed to be about $\mu = 2.0$, thus making foot slipping rare. A *NaturalPoint*^{TM} FLEX V100 IR camera is mounted above the air table. The camera provides positions of all IR reflectors to a PC, which communicates with the robot over wireless XBee protocol. Mechanism and environment parameters are given in Table I.

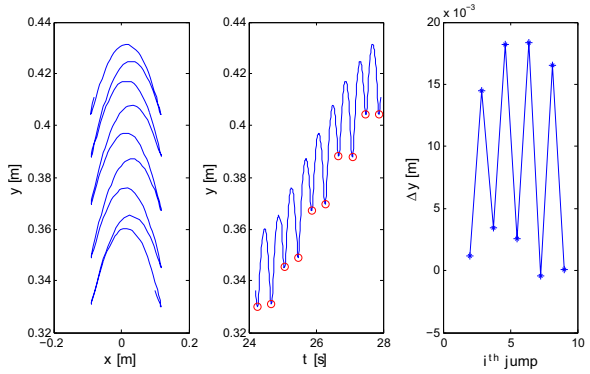

(a) Period-2

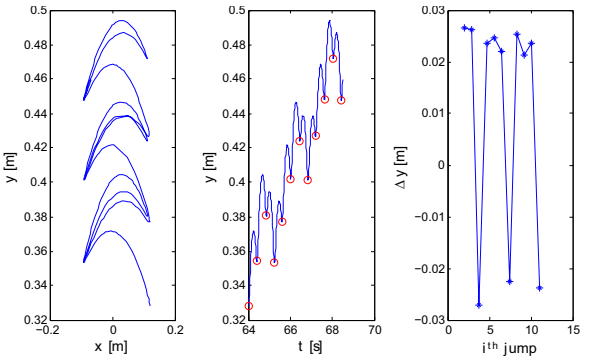

(b) Period-4

Fig. 10. Experimental data of open-loop climbing: climbing trajectory (left column), height y vs. time (middle column), where the red circle indicates the Poincaré section, and Δy between pairs of consecutive states on Poincaré section (right column). (a) Stable period-2 climbing up. (b) Stable period-4 climbing up.

B. Open-loop experimental results

The goal of the open-loop experiments was to verify our analysis results, particularly the existence of period-1, period-2, and period-4 stable cycles, and the correlation of stability with input energy. We readily observed stable period-2 and period-4 motions (Fig. 10), but not period-1 motions, perhaps due to the asymmetric leg angles noted earlier. To measure stability we use Mean Jumps To Failure (MJTF), similar to [28]. We chose ten different energy levels and ran eight experiments for each energy level. For each individual experiment, we counted the number of jumps before crash, as seen in Fig. 11. This plot correlates to our simulation results in Fig. 8, showing how the system is more stable when the input energy is increased. Typically the main failure mode is the body orientation drifting to the point where the state of the robot exits the basin of attraction.

C. Closed-loop experimental results

The goal of the closed-loop experiments was to assess the feasibility of stabilizing the vertical height of the robot. We determine height error from IR tracker data at the Poincaré section (at touch down), and use a PID controller to determine energy input for the next touch down. Fig. 12 shows the successful stabilization at a height of 55 cm. See supplementary attachment for a video of this experiment.

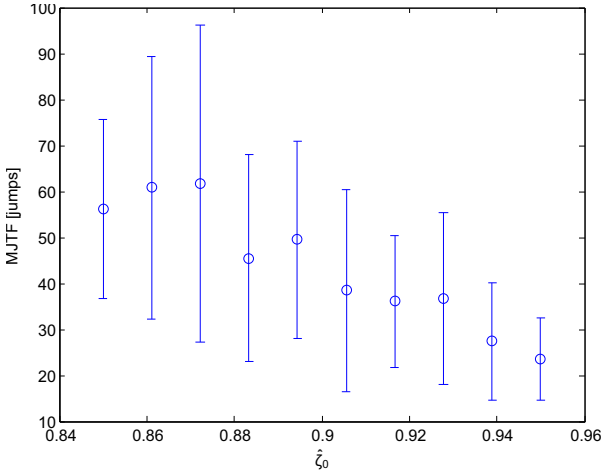

Fig. 11. Mean Jumps To Failure (MJTF) vs. leg retraction $\hat{\zeta}_0$. Vertical axis shows the average number of jumps before crash, with error bars representing the standard deviation. Leg retraction $\hat{\zeta}_0$ was roughly approximated. Eight experiments are conducted for each energy level.

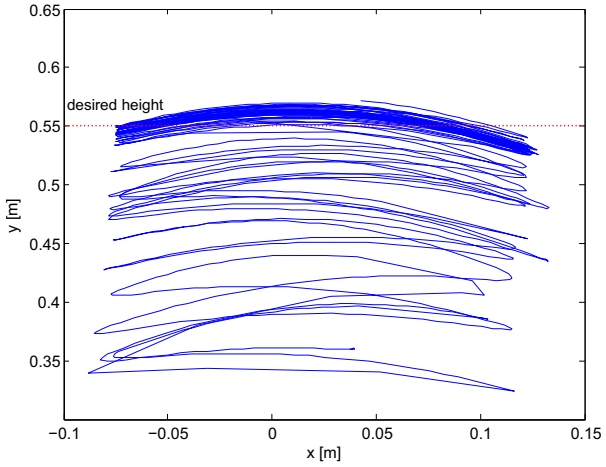

(a) Trajectory

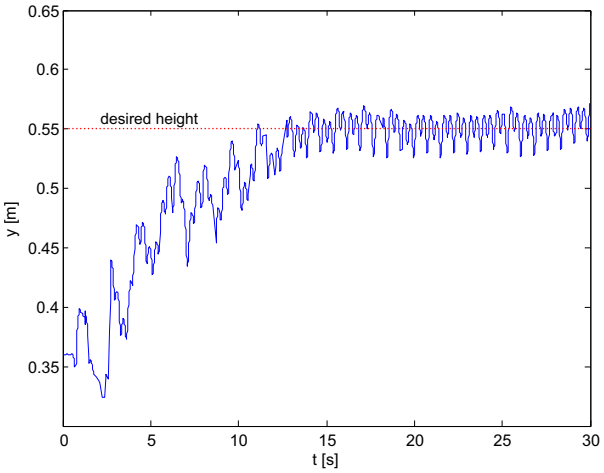

(b) Height vs. time

Fig. 12. Experimental data of closed-loop climbing reaching a desired height of 55 cm: (a) climbing trajectory; (b) height y vs. time.

D. Discussion

While there is qualitative agreement between simulation, analysis, and experiment, there are also differences arising from modeling approximations and the limitations of our experimental apparatus. While we model the robot body as a point mass, the actual robot body has pitch which drifts, ultimately leading to failure when leg angles reach joint limits. We have already noted the asymmetry in the robot mechanism, which may be responsible for the lack of observed period-1 stable gaits. We also lack an accurate launching mechanism. Finally, since the most stable gaits involve the most rapid climbing, our most successful experiments are limited by the height of tilted table.

VII. Conclusions

This paper demonstrates the use of dynamic leaping maneuvers of a two legged robot to traverse up a vertical channel. By storing elastic energy in the springy legs during flight phase the robot is able to kick off and release this energy during impact with the walls. We use a simplified SLIP model to understand the dynamics and stability of the robot and show correlation to experiments. Currently, our prototype is able to achieve a relatively simple task of climbing inside a chute in a reduced gravity, planar environment. We intend to continue and push the capabilities of the ParkourBot to climb in more complex environments such as ones with random footholds at different orientations while controlling foot placement. To do so, we intend to further test different spring materials, different thrust mechanisms and enhance the control capabilities of the mechanism.

VIII. Acknowledgments

We would like to thank Garth Zeglin for the use of his explanations of the BowLeg concept, and Andrew Long, Nelson Rosa, and Tsahai Philip. Thanks to Ken Goldberg for early discussions on the possibility of robot parkour.

References

[1] H. B. Brown, Jr. and G. Zeglin, "The Bow Leg hopping robot," in *IEEE International Conference on Robotics and Automation*, 1998, pp. 781–786.

[2] G. Zeglin, "The Bow Leg hopping robot," Ph.D. dissertation, Robotics Institute, Carnegie Mellon University, Pittsburgh, PA, October 1999.

[3] A. Degani, H. Choset, and M. T. Mason, "DSAC – Dynamic, Single Actuated Climber: Local stability and bifurcations," in *Proc. of the IEEE International Conference on Robotics and Automation, (ICRA)*, 2010.

[4] A. Degani, A. Shapiro, H. Choset, and M. T. Mason, "A dynamic single actuator vertical climbing robot," in *Proc. of IEEE/RSJ International Conference on Intelligent Robots and Systems (IROS'07)*, 2007.

[5] M. H. Raibert and H. B. Brown, Jr., "Experiments in balance with a 2D one-legged hopping machine," *ASME Journal of Dynamic Systems, Measurement, and Control*, vol. 106, pp. 75–81, 1984.

[6] M. H. Raibert, H. B. Brown, Jr., and M. Chepponis, "Experiments in balance with a 3D one-legged hopping machine," *International Journal of Robotics Research*, vol. 3, pp. 75–92, 1984.

[7] G. Zeglin and H. B. Brown, Jr., "Control of a Bow Leg hopping robot," in *IEEE International Conference on Robotics and Automation*, 1998, pp. 793–798.

[8] M. H. Raibert, *Legged Robots That Balance*. Cambridge, MA: The MIT Press, 1986.

[9] R. Blickhan, "The spring-mass model for running and hopping," *Journal of Biomechanics*, vol. 22, pp. 1217–1227, 1989.

[10] R. Blickhan and R. J. Full, "Similarity in multilegged locomotion: Bouncing like a monopode," *Journal of Comparative Physiology*, vol. 173, pp. 509–517, 1993.

[11] M. Garcia, A. Chatterjee, A. Ruina, and M. Coleman, "The simplest walking model: stability, complexity, and scaling," *Journal of Biomechanical Engineering*, vol. 120, no. 2, pp. 281–288, Apr. 1998.

[12] A. D. Kuo, "Energetics of actively powered locomotion using the simplest walking model," *Journal of Biomechanical Engineering*, vol. 124, no. 1, pp. 113–120, Feb. 2002.

[13] U. Saranli, M. Bühler, and D. E. Koditschek, "RHex: A simple and highly mobile hexapod robot," *International Journal of Robotics Research*, vol. 20, no. 7, pp. 616–631, 2001.

[14] T. Allen, R. D. Quinn, R. J. Bachmann, and R. E. Ritzman, "Abstracted biological principles applied with reduced actuation improve mobility of legged vehicles," in *IEEE/RSJ International Conference on Intelligent Robots and Systems*, 2003, pp. 1370–1375.

[15] S. A. Bailey, J. G. Cham, M. R. Cutkosky, and R. J. Full, "Comparing the locomotion dynamics of the cockroach and a shape deposition manufactured biomimetic hexapod," in *Experimental Robotics VII, Lecture Notes in Control and Information Sciences*. Springer, 2001, pp. 239–248.

[16] D. Longo and G. Muscato, "The Alicia^3 climbing robot," *IEEE Robotics and Automation Magazine*, vol. 13, pp. 2–10, 2006.

[17] A. Shapiro, E. Rimon, and S. Shoval, "PCG: A foothold selection algorithm for spider robot locomotion in 2D tunnels," *The International Journal of Robotics Research*, vol. 24, no. 10, pp. 823–844, 2005.

[18] A. Greenfield, A. A. Rizzi, and H. Choset, "Dynamic ambiguities in frictional rigid-body systems with application to climbing via bracing," in *Proc. of the IEEE International Conference on Robotics and Automation, (ICRA)*, Barcelona, Spain, 2005, pp. 1947– 1952.

[19] T. Bretl, "Motion planning of multi-limbed robots subject to equilibrium constraints: The free-climbing robot problem," *The International Journal of Robotics Research*, vol. 25, no. 4, pp. 317–342, 2006.

[20] S. Kim, M. Spenko, S. Trujillo, B. Heyneman, V. Mattoli, and M. R. Cutkosky, "Whole body adhesion: hierarchical, directional and distributed control of adhesive forces for a climbing robot," in *IEEE International Conference on Robotics and Automation*, 2007, pp. 1268–1273.

[21] M. Murphy and M. Sitti, "Waalbot: An agile small-scale wall climbing robot utilizing pressure sensitive adhesives," *IEEE/ASME Trans. on Mechatronics*, vol. 12, no. 3, pp. 330–338, 2007.

[22] K. Autumn, M. Buehler, M. Cutkosky, R. Fearing, R. J. Full, D. Goldman, R. Groff, W. Provancher, A. A. Rizzi, U. Saranli, A. Saunders, and D. E. Koditschek, "Robotics in scansorial environments," in *Proc. of SPIE Vol. 5804 Unmanned Ground Vehicle Technology VII*, 2005, pp. 291–302.

[23] S. Kim, A. T. Asbeck, M. R. Cutkosky, and W. R. Provancher, "SpinybotII: Climbing hard walls with compliant microspines," in *Proc. of the 12th International Conference on Advanced Robotics, (ICAR '05)*, Seattle, WA, 2005, pp. 601–606.

[24] J. Clark, D. Goldman, P. Lin, and G. Lynch, "Design of a Bio-inspired Dynamical Vertical Climbing Robot," *Robotics: Science and Systems III Atlanta, Georgia*, 2007.

[25] S. Jensen-Segal, S. Virost, and W. Provancher, "ROCR: Dynamic vertical wall climbing with a pendular two-link mass-shifting robot," in *IEEE International Conference on Robotics and Automation, (ICRA)*, 2008, pp. 3040–3045.

[26] H. B. Brown, Jr., G. Zeglin, and I. R. Nourbakhsh, "Resilient leg design for hopping running and walking machines," Patent, Sept., 2007, US 7,270,589 B1.

[27] P. Gill, W. Murray, and M. Wright, "The levenberg-marquardt method," *Practical Optimization*, pp. 136–137, 1981.

[28] K. Byl and R. Tedrake, "Metastable walking machines," *The International Journal of Robotics Research*, vol. 28, no. 8, p. 1040, 2009.